Kotov Nicholas A. (Orcid ID: 0000-0002-6864-5804)

Chirality

Plasmonic Nanoparticles Assemblies Templated by Helical Bacteria and Resulting Optical Activity

Wenchun Feng[1,3,4], Usha Kadiyala[2,3], Jiao Yan[3,4], Yichun Wang[3,5], Victor J. DiRita[6], J. Scott VanEpps[2,3,5,7,8], Nicholas A. Kotov[a]

Abstract: Plasmonic nanoparticles (NPs) adsorbing onto helical bacteria can lead to formation of NP helicoids with micron scale pitch. Associated chiroptical effects can be utilized as bioanalytical tool for bacterial detection and better understanding of the spectral behavior of helical self-assembled structures with different scales. Here we report that enantiomerically pure helices with micron scale of chirality can be assembled *Campylobacter jejuni*, a helical bacteria known for severe stomach infections. These organisms have right-handed helical shapes with a pitch of 1–2 microns and can serve as versatile templates for a variety of NPs. The bacteria itself shows no observable rotatory activity in the visible, red and near-IR ranges of electromagnetic spectrum. The bacterial dispersion acquires chiroptical activity at 500–750 nm upon plasmonic functionalization with Au NPs. Finite-difference time-domain simulations confirmed the attribution of the chiroptical activity to the helical assembly of gold nanoparticles. The position of the circular dichroism peaks observed for these chiral structures overlaps with those obtained before for Au NPs and their constructs with molecular and nanoscale chirality. This work provides an experimental and computational pathway to utilize chiroplasmonic particles assembled on bacteria for bioanalytical purposes.

Keywords: bacteria, circular dichroism, plasmonic, gold nanoparticle, *C. jejuni*, simulation, plasmonic, mesoscale, biotechnology

Introduction

Chirality is one of the most universal properties of the physical world.[1–4] Chiral nanoscale structures from inorganic materials with strongly polarizable plasmonic and excitonic electronic states, provide an avenue to efficiently manipulate polarization of light.[5–14] Templated assemblies of plasmonic nanoparticles (NPs) using biomacromolecules can produce superstructures with nanoscale chiral geometries.[14–20] However, the assemblies with micron-scale chiral geometries expected to be formed on live or dormant helical microorganisms would also be interesting. This research effort should extend scaling behavior for chiroptical properties of plasmonic structures to microscale. Furthermore, self-assembly of NPs[21,22] into helices using biological templates may in perspective circumvent the problems of three-dimensional lithography,[9,23,24] such as low throughput, due to efficient template assembly at the interfaces.[25] The assemblies of NPs on microscale organisms would also be interesting as a new experimental tool to observe the dynamics of the microorganisms. Last but not the least, the emergence of the chiroptical activity in the part of the spectrum where the biological structures typically have no noticeable circular dichroism peaks can also be utilized for rapid detection of bacterial infections.

Bacteria exhibit a wide range of sizes (usually on the micron scale) and shapes,[26] from spheres and rods of no apparent chirality to chiral asymmetric spirals such as those of *Campylobacter jejuni*. In practical applications, the existence of chirality itself is not necessarily sufficient for its utilization in polarization-based devices. Many artificial systems are inherently racemic and chiroptically inactive, meaning that they exist as an equal amount of left- and right-handed species, which cancel out each other's optical activity. A chiroptical system must display enantiomeric excess (e.e.), where one species' handedness is dominant over the other in order to be chiroptically active in a specific region of electromagnetic

[a] *Corresponding Author*
Prof. Nicholas A. Kotov
Biointerfaces Institute, Department of Chemical Engineering, Department of Biomedical Engineering
University of Michigan
Ann Arbor, MI 48109
Fax: (+1) 7347638768
E-mail: kotov@umich.edu

1 Current Address: US Food and Drug Administration, Silver Spring, MD 20993
2 Department of Emergency Medicine, University of Michigan, Ann Arbor, MI 48109
3 Biointerfaces Institute, University of Michigan, Ann Arbor, MI 48109
4 Department of Chemical Engineering, University of Michigan, Ann Arbor, MI 48109
5 Department of Biomedical Engineering, University of Michigan, Ann Arbor, MI 48109
6 Department of Microbiology and Molecular Genetics, Michigan State University, East Lansing, MI 48824
7 Michigan Center for Integrative Research in Critical Care, University of Michigan, Ann Arbor, MI 48109
8 Macromolecular Science and Engineering Program, University of Michigan, Ann Arbor, MI 48109

Received: ((will be filled in by the editorial staff))
Revised: ((will be filled in by the editorial staff))
Published online: ((will be filled in by the editorial staff))

spectrum.[22,27,28] Asymmetric bacteria are nearly idea experimental system in this case because they are enantiopure chiral microstructures. Both *Campylobacter jejuni (C. jejuni)*[29] and *Leptospira interrogans*[30] are known to have right-handed twist. Colonies of *Bacillus subtilis* are known to form right-handed microfibers at room temperature.[31]

There have been extensive studies using light to interrogate bacterial systems for their volumetric organism density by visible and near-infrared (NIR) light absorption, scattering, or diffraction.[32–40] However, despite the prevalence of chirality in bacteria, the implication of their microscale chirality for optical properties are not yet well understood and their enantiopure nature is technologically underutilized.[41–43] NP functionalization has been previously conducted on a variety of bacteria species,[44–46] but until now, there have been no studies on plasmonic functionalization on chiral bacteria and associated chiroptical activity. In this work, we report plasmonic functionalization of *C. jejuni* and finite-difference time-domain (FDTD) simulations of their circular dichroism (CD) spectra that not only confirmed the expectation of the formation of microscale template helicoids, but also show conformal Au NP shell enhance the chiroptical response. Overall, this study contributes to further understanding of chiroptical properties of helical bacteria; the findings can be used to advance chiral photonics and rapid detection of bacterial infections.

Materials and Methods

Synthesis of Au NPs: Positively and negatively charged Au NPs in aqueous dispersions were synthesized according to previously published protocols with 2-aminoethanethiol and citrate as ligands, respectively.[47,48] Their UV-Vis absorption spectra (Figure S1) were obtained using an Agilent/HP 8453 UV-Vis spectrophotometer, and their size and molar concentration were determined according to methods described by Khlebstov[49] and Liu[50] (positively charged Au NPs: 33 nm, 6.75×10^{-10} M; negatively charged Au NPs: 11 nm, 1.22×10^{-8} M).

Synthesis of Au Nanorods (NRs): The synthetic procedure was adapted with some modification from a method reported by Nikoobakht.[51] Preparation of Au seed solution: cetyltrimethylammonium bromide (CTAB)-capped seeds were prepared by chemical reduction of HAuCl4 with NaBH4: Freshly prepared, ice-cold NaBH4 (0.01 M, 10 mL) was injected into a mixture of CTAB (0.1 M, 7.5 mL), HAuCl4 (23 mM, 0.1 mL) and deionized water (1.8 mL) under magnetic stirring for 3 min. The color of the solution turned from yellow to brown, indicating the formation of Au seeds. The seed solution was kept undisturbed at 30°C for 2–5 h before use.

Growth of Au NRs: The Au NRs growth solution was made by mixing CTAB (0.1 M, 100 mL), HAuCl4 (25 mM, 2 mL), AgNO3 (0.1 M, 120 µL), and ascorbic acid (AA, 0.1 M, 552 µL). The seed solution (120 µL) was added to the growth solution to initiate the growth of Au NRs. The well-mixed solution was kept undisturbed for 12 h, then AA (0.1 M, 552 µL) was added twice at 40 min intervals. The total reaction time was 24 h.

Plasmonic functionalization: For positively charged Au NP functionalization, 1.25 mL *C. jejuni* (NCTC 11168, wild type clinical strain) aqueous solution (OD = 2.5) was mixed with 5 mL Au NP solution, and incubated for 10 min followed by a centrifuge step at 4000 rpm for 5 min. The precipitate was redispersed in 1.25 mL water and then used for CD spectroscopy. For negatively charged Au NP functionalization, the first step was to coat the bacteria with a layer of polydiallyldimethylammonium (PDDA), since the bacteria surface is negatively charged and the PDDA layer alters the surface charge to positive making it possible for the adsorption of negatively charged Au NPs. 1.25 mL *C. jejuni* aqueous solution (OD = 2.5) was mixed with 5 mL PDDA (1 mg/mL, in 0.1 M NaCl) solution, and incubated for 10 min, followed by a centrifuge step at 4000 rpm for 30 min. Then the precipitate was washed 3 times with 6.25 mL water at 4000 rpm for 15 min. Finally, the precipitate was redispersed in 1.25 mL water and mixed with 10 mL Au NP solution. This solution was allowed to incubate for 5 min before placing in a centrifuge at 4000 rpm for 5 min and then used for CD measurements.

CD measurements: JASCO J-815 CD spectrophotometer was used for CD spectroscopy with the following scanning parameters: Scanning speed = 100 nm/min, data pitch = 0.1 nm, D.I.T. = 4 s, bandwidth = 1 nm, number of accumulation = 1.

Scanning electron microscopy (SEM) imaging: After CD measurements, the bacteria solutions were subject to glutaraldehyde fixing and ethanol dehydration gradients. The final dehydrated sample solution was drop cast on a silicon wafer and imaged without sputter coating in SEM (FEI Nova 200 Nanolab SEM/FIB).

FDTD simulations: The CD, extinction, and g factor spectra were calculated using a commercial FDTD software package (Lumerical Solutions Inc., http://www.lumerical.com/tcad-products/fdtd/). The structural model of the bacteria was constructed from Figure 1a in COMSOL with the following parameters: Shape = helix, number of turns = 1, major radius = 112 nm, minor radius = 139 nm, axial pitch = 1300 nm, radial pitch = 0 nm, right-handed chirality and end caps are perpendicular to spine. This model was then imported to 3ds Max, where Au NPs of 11 nm diameter were added onto the surface of the bacteria with a spacing of 28 nm between the center of each NP corresponding to the distances between the NPs observed in the samples by electron microscopy. The mesh type is auto non-uniform with a mesh size of 1.5 nm along all three axes and a mesh accuracy of 3. The circularly polarized light irradiation is along the axial direction of the helical model structure. Simulation environment was in water (nwater = 1.33). The refractive index of *C. jejuni* was estimated from that of E. coli. (1.388).[52] Refractive index of Au is derived from Johnson and Christy (LUMERICAL database).[53]

Results and Discussion

SELF-ASSEMBLY OF NANOSCALE COLLOIDS ON BACTERIAL SURFACE

C. jejuni is a helical bacterium with a curvy rod shape (Figure 1a), and is one of the most common causes of gastroenteritis around the globe.[54,55] At the onset of the study we hypothesized that this bacteria can be used as a template for the self-assembly of the plasmonic NPs or other nanoscale colloids, such as nanorods (NRs) into helices that should lead to chiroptical activity in the red part of the spectrum. The challenge for this project was successful deposition of the NPs or NRs on to the bacterium while retaining its curvy rod shape. Note that helical shape is typical only for live *C. jejuni* and they convert to mostly achiral rod-like shape under stress.

Self-assembly on bacterial surface was carried out for of positively and negatively charged Au nanocolloids. Since the surface of bacteria are typically negatively charged, we started with the direct adsorption of positively charged NPs. However, we observed non-uniform deposition of the NPs attributed to the uneven charge distribution on the bacterial surfaces (Figure 1b).[45]

Deposition of the negatively charged NPs followed a layer-by-layer (LBL) assembly that was previously successful in coating bacteria.[44–46,56–57] After one layer of polydiallyldimethylammonium (PDDA) deposition on the bacteria, the negatively charged Au NPs can then be completely deposited on top of PDDA. The PDDA layer imparted a uniform positive charge (zeta potential shown in Figure S2) throughout the surface of the bacteria, and the subsequent negatively charged Au NPs adsorbed onto this layer with much higher uniformity compared to those of the positively charged Au NPs (Figure 1c,d). The uniformity of the coating is particularly significant in the light of subsequent modeling of the chiroptical properties of these particulate helicoids.

other bacteria species is unknown, therefore we approximated the refractive index of *C. jejuni* with that of *E. coli* (1.388). Considering that bacteria mostly consist of water which should lead to a refractive index close to that of water at 1.33, the approximation most likely holds true. Although *C. jejuni* is a helical bacterium, because its refractive index is close to that of water, there is no rotatory power in the visible region for bacterial dispersion (Figure 2a). There is chiroptical activity in the UV region (200–400 nm) due to the proteins and other biomolecular components in the bacterium; however, this chiroptical activity is not specific to the bacteria, making the analysis of the corresponding CD spectra from various bacterial species less informative than for, say individual amino acids, drug enantiomers, or chiral NPs.

After plasmonic functionalization with either positively or negatively charged Au NPs, the bacteria acquired detectable rotatory power in the visible region of electromagnetic spectrum between 500 and 750 nm, which, of course, was not observed before in any bacterial species. The chiroptical response for both types of Au NPs is positive and the chiral anisotropy (g) factor is around 1×10^{-4} and 2×10^{-4} for positively and negatively charged Au NPs, respectively.

The question now is what scale of chirality these CD peaks can be attributed to. They may originate from the local enhancement of CD activity of the chiral biomolecules due to the weak but noticeable hybridization of excitonic and plasmonic states on biomolecules and NPs.[58] To answer this question, symmetrically shaped bacteria, namely *Escherichia coli* and *Staphylococcus aureus*, were coated with positively charged Au NPs following the same procedure, but none of the products showed any observable chiroptical activity from 500 to 750 nm within the

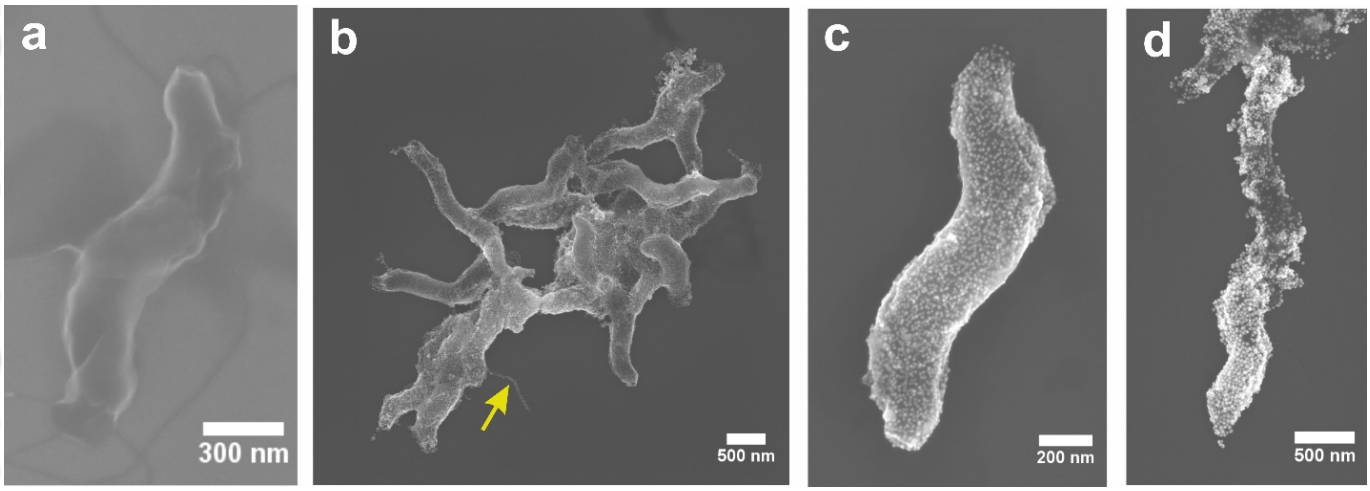

Figure 1. SEM images of (a) *C. jejuni*, (b)-(c) coated with negatively charged Au NPs (yellow arrow points to a coated flagellum), and (d) coated with positively charged Au NPs.

OPTICAL PROPERTIES

Looking into the optical properties of the bacterium-templated NP assemblies, except for *E. coli*, the refractive index for most

sensitivity of the state-of-the-art instrumentation for chiroptical measurements (Figure S3). This indicated that this CD peak does not correspond to the chiroplasmonic activity of local complexes of NP with proteins or other biomolecules. This experiment also showed the necessity of the curvy rod shape of *C. jejuni* for the induction of rotatory power at the 500-70 nm CD band.

The chiroptical activity between the coatings made from positively and negatively charged NPs is similar, though the positively charged Au NPs coated bacteria showed a slightly

higher scattering background in the absorption spectrum compared to the negatively charged ones (Figure 2b). Again, this fact is likely to be attributed to some degree of aggregation of the bacteria because the NP layer can increase supramolecular and electrostatic attraction between two or more organisms. One also need to consider that positively charged NPs adsorb directly on to the surface of bacteria which is likely to have uneven charge distribution, while the negative Au NPs attach onto the relative uniform charged surface primed by PDDA. Notably the overall chiroptical activity is relatively weak, which is associated with the mismatch between the characteristic pitch of *C. jejuni* in the micron range and the submicron wavelengths of photons in the visible part of the spectrum available for measurements at the moment. Although the weakness of the visible response is somewhat discouraging, the data presented in Figures 1,2 provide proof–of-concept for the formation of chiroptically active superstructures using the convenient shape of bacteria. The prior studies on chiral nano- and mesoscale structures indicate that once the origin of the CD peaks is uncovered, it can be further enhanced by numerous means for analytical and other purposes.

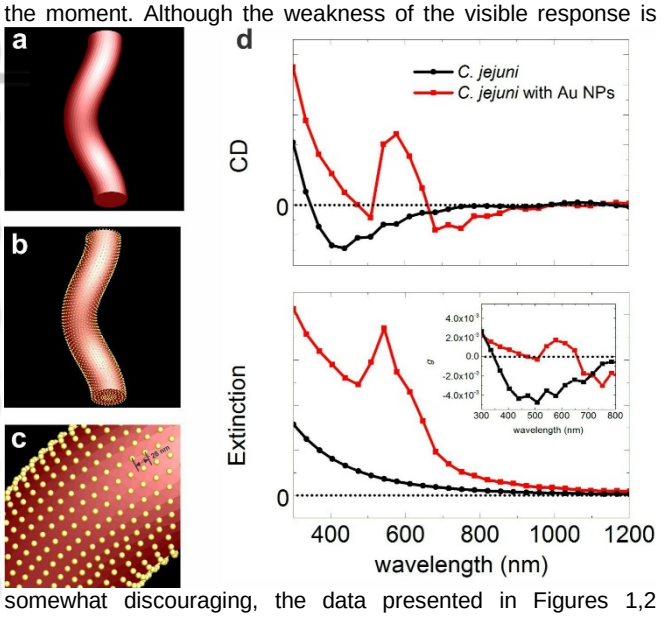

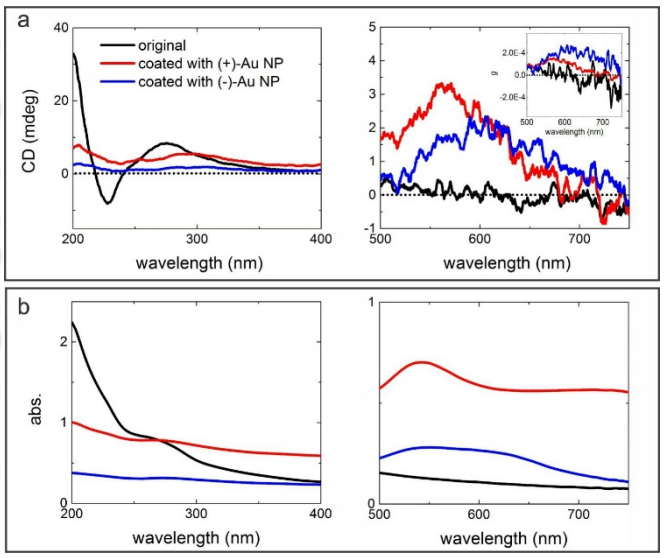

Figure 2. (a) CD and (b) absorbance spectra in UV (left graphs) and visible (right graphs) parts of the spectrum for *C. jejuni* before and after being coated with positively or negatively charged Au NPs. Inset in the CD spectrum for the visible spectral part shows the corresponding g-factor spectra.

To confirm generality of the observed chiroptical response and its spectral tunability, *C. jejuni* were also coated with Au NRs. These test samples also exhibited moderate chiroptical response (~4 mdeg) at wavelengths futher in the red part of the electromagnetic spectrum, namely between 600 and 700 nm, corresponding to plasmonic resonance for Au NRs (Figure S4a–b). This indicates broad applicability in terms of the functionalizing nanomaterials that can be used on the surface of *C. jejuni*. Futhermore, Au NR coating on chiral templates are known to enhance CD apmlitudes copared to Au NPs due to stronger plasmon-plasmon interactions.[59] Futher methods of enhancement of the chiroptical activity can be related to better preservation of the curvy shape of the bacteria that may be damaged (Figure S4c) by the CTAB surfactant on the Au NRs.[60]

SIMULATIONS

Simulations can also confirm the origin of the chiroptical activity and determine the methods for further augmentation of the bacteria's CD spectra. A conformal layer of NPs similar to the one observed in Figure 1C lead to distinct CD peak in the plasmonic part of the spectrum (Figure 3) whose position matches that observed experimentally. Simulations also revealed that a complete layer of Au coating around *C. jejuni* can afford the IR part of the spectrum with great amplitude of polarization rotation (Figure S5). Bacteria coated with the NP shell exhibited significantly higher chiroptical response due to the overall shape compared to other sources of chiroptical activity[5] due to stronger field coupling between the Au NPs.

Figure 3. Simulation model of (a) *C. jejuni* and (b) *C. jejuni* coated with Au NPs with a magnified view in (c). (d) Simulated CD and extinction spectra of *C. jejuni* with and without Au NPs coating. Inset shows the calculated g-factor spectra.

Conclusion

Helical bacteria, either as individual cells, can be used as to guide self-assembly of plasmonic nanocomponents toward the formation of enantiopure helicoids circumventing the problem of subtlety of chiral interactions known from chiral chemistry. We found that the chiroptical activity of the Au NP assemblies with mesoscale chiral geometries templated by *C. jejuni* are similar to those with nanoscale and molecular scale chirality, which is related to the dominance of the plasmonic absorption for CD bands in the visible and near infrared parts of the spectrum. While functionalization of helical bacteria with nanoscale colloids, such as NPs and NRs, may provide a biotechnological pathway for the templating mesoscale chiroplasmonic structures, it is not likely to compete with lithography. However, it may be suitable for bacterial detection which acquires increasing significance both with the microbiome studies and the rise of antibiotic resistance. Furthermore, these studies also open the door to new applications of chiroplamonic effects for monitoring of shape changes of bacteria [63–65] and time-resolved studies of NP interactions with bacteria[61,62]. Extension of the spectral window of chiroptical spectroscopy to far-IR or terahertz[66] spectral range

will further increase the sensitivity due to the stronger polarization rotation for longer wavelengths.

Acknowledgements

The authors would like to thank the University of Michigan's Michigan Center for Materials Characterization for its assistance with scanning electron microscopy. The central part of this work was supported by the NSF-funded project "Energy- and cost-efficient manufacturing employing nano-particles" (grant no. 1463474) and the Air Force Office of Scientific Research–funded project "Nanocomposite ion conductors from branched aramid nanofibers" (grant no. FA9550-16-1-0265). Additional support acknowledged to NIH K08 AI128006.

Supporting information

Additional supporting information may be found in the online version of this article at the publisher's website.

REFERENCES AND NOTES

1. Nakanishi, K. & N. Berova, R. W. W. *Circular Dichroism: Principles and Applications*. (Wiley-VCH, 2000).
2. Miles, A. J., Whitmore, L. & Wallace, B. A. Spectral magnitude effects on the analyses of secondary structure from circular dichroism spectroscopic data. *Protein Sci.* **14**, 368–74 (2005).
3. Yeom, J. Santos, U., Chekini, M. Cha, M. de Moura, A.F.. Kotov, N.A.. Chiromagnetic Nanoparticles and Gels, Science, **359**, 309-314 (2018).
4. Morrow, S. M., Bissette;, A. J. & Fletcher, S. P. Transmission of chirality through space and across length scales. *Nat. Nanotechnol.* **12**, 410–419 (2017).
5. Ma, W. *et al.* Chiral Inorganic Nanostructures. *Chem. Rev.* **117**, (2017).
6. Guerrero-Martínez, A., Alonso-Gómez, J. L., Auguié, B., Cid, M. M. & Liz-Marzán, L. M. From individual to collective chirality in metal nanoparticles. *Nano Today* **6**, 381–400 (2011).
7. Xia, Y., Zhou, Y. & Tang, Z. Chiral inorganic nanoparticles: origin, optical properties and bioapplications. *Nanoscale* **3**, 1374 (2011).
8. Oaki, Y. & Imai, H. Amplification of chirality from molecules into morphology of crystals through molecular recognition. *J. Am. Chem. Soc.* **126**, 9271–9275 (2004).
9. Mark, A. G., Gibbs, J. G., Lee, T.-C. & Fischer, P. Hybrid nanocolloids with programmed three-dimensional shape and material composition. *Nat. Mater.* **12**, 802–7 (2013).
10. Zhou, Y. *et al.* Biomimetic Hierarchical Assembly of Helical Supraparticles from Chiral Nanoparticles. *ACS Nano* **10.1021/ac**, (2016).
11. Singh, G. *et al.* Self-assembly of magnetite nanocubes into helical superstructures. *Science* **345**, 1149–53 (2014).
12. Duan, Y. *et al.* Angewandte Optically Active Nanostructured ZnO Films. *Angew* **54**, 15170–15175 (2015).
13. Kim, Y. *et al.* Reconfigurable chiroptical nanocomposites with chirality transfer from the macro- to the nanoscale. *Nat. Mater.* **15**, 461–468 (2016).
14. Yan, Jiao; Feng, Wenchun; Kim, Ji-Young; Lu, Jun; kumar, prashant; Mu, Zhengzhi; Wu, Xiaochun; Mao, Xiaoming; Kotov, Nicholas Self-Assembly of Chiral Nanoparticles into Semiconductor Helices with Tunable Near-Infrared Optical Activity, Chemistry of Materials, **32**, 1, 476-488 (2020).
15. Lan, X. *et al.* Au nanorod helical superstructures with designed chirality. *J. Am. Chem. Soc.* **137**, 457–62 (2015).
16. Chen, W. *et al.* Nanoparticle superstructures made by polymerase chain reaction: Collective interactions of nanoparticles and a new principle for chiral materials. *Nano Lett.* **9**, (2009).
17. Mastroianni, A. J. Pyramidal and chiral grouping of gold nanocrystals assembled using DNA scaffolds. *J. Am. Chem. Soc.* **131**, (2010).
18. Hou, K. *et al.* Optically Active Inverse Opal Photonic Crystals. *J. Am. Chem. Soc.* **140**, 16446–16449 (2018).
19. Lv, J. *et al.* Biomimetic Chiral Photonic Crystals. *Angew. Chem. Int. Ed.* **58**, 7783–7787 (2019).
20. Lv, J. *et al.* Gold Nanowire Chiral Ultrathin Films with Ultrastrong and Broadband Optical Activity. *Angew. Chem. Int. Ed.* **56**, 5055–5060 (2017).
21. Yeom, J. *et al.* Chiral templating of self-assembling nanostructures by circularly polarized light. *Nat. Mater.* **14**, 66–72 (2015).
22. Feng, W. *et al.* Assembly of mesoscale helices with near-unity enantiomeric excess and light-matter interactions for chiral semiconductors. *Sci. Adv.* **3**, e1601159 (2017).
23. Gansel, J. K. *et al.* Gold helix photonic metamaterial as broadband circular polarizer. *Science* **325**, 1513–5 (2009).
24. Esposito, M. *et al.* Triple-helical nanowires by tomographic rotatory growth for chiral photonics. *Nat. Commun.* **6**, 6484 (2015).
25. Kotov, N. A. Self-assembly of inorganic nanoparticles: Ab ovo. *Europhys. Lett.* **119**, 66008 (2017).
26. Hug, L. A. *et al.* A new view of the tree and life's diversity. *Nat. Microbiol.* **1:16048**, (2016).
27. Zhang, J. *et al.* Multiscale deformations lead to high toughness and circularly polarized emission in helical nacre-like fibres. *Nat. Commun.* **7**, 10701 (2016).
28. Sun, H. *et al.* Homochiral columns constructed by chiral self-sorting during supramolecular helical organization of hat-shaped molecules. *J. Am. Chem. Soc.* **136**, 7169–7185 (2014).
29. Fields, P. & Fitzgerald, C. Campylobacter jejuni. (2004).
30. Carleton, O., Charon, N. W., Allender, P. & O'Brien, S. Helix handedness of Leptospira interrogans as determined by scanning electron microscopy. *J. Bacteriol.* **137**, 1413–1416 (1979).
31. Mendelson, N. H. & Karamata, D. Inversion of helix orientation in Bacillus subtilis macrofibers. *J. Bacteriol.* **151**, 450–454 (1982).
32. Ferrari, G. M. & Tassan, S. A method for the experimental determination of light absorption by aquatic heterotrophic bacteria. *J. Plankt. Res.* **20**, 757–766 (1998).
33. Katz, A. *et al.* Bacteria Size Determination by Elastic Light Scattering. *IEEE J. Sel. Top. Quantum Electron.* **9**, 277–287 (2003).
34. Xu, M. & Katz, A. Statistical interpretation of light anomalous diffraction by small particles and its applications in bio-agent detection and monitoring. in *Light Scattering Reviews 3* 27–67 (Springer, 2008). doi:10.1007/978-3-540-48546-9
35. Balch, W. M. *et al.* Fundamental Changes in Light Scattering Associated with Infection of Marine Bacteria by Bacteriophage. *Limnol. Oceanogr.* **47**, 1554–1561 (2002).
36. Sânchez, O. & Mas, J. Light absorption by phototrophic bacteria: Effects of scattering, cell concentration and size of the culture vessel. *Int. Microbiol.* **2**, 233–240 (1999).
37. Waltham, C., Boyle, J., Ramey, B. & Smit, J. Light

scattering and absorption caused by bacterial activity in water. *Appl. Opt.* **33**, 7536–40 (1994).
38. Ulloa, O., Sathyendranath, S., Platt, T. & Quiñones, R. A. Light scattering by marine heterotrophic bacteria. *J. Geophys. Res.* **97**, 9619–9629 (1992).
39. Krepelka, P., Martos, F. C., Posada-Izquierdo, G. D. & Pérez-Rodríguez, F. Measuring and application of NIR light absorption coefficient of bacteria. in *Progress in Electromagnetics Research Symposium* 2336–2339 (2014).
40. Bateman, J. B., Wagman, J. & Carstensen, E. L. Refraction and absorption of light in bacterial suspensions. *Kolloid-Zeitschrift und Zeitschrift für Polym.* **208**, 44–58 (1966).
41. Wang, S., Furchtgott, L., Huang, K. C. & Shaevitz, J. W. Helical insertion of peptidoglycan produces chiral ordering of the bacterial cell wall. *Proc. Natl. Acad. Sci. U. S. A.* **109**, E595–E604 (2012).
42. Ben-Jacob, E. *et al.* Cooperative formation of chiral patterns during growth of bacterial colonies. *Phys. Rev. Lett.* **75**, 2899–2902 (1995).
43. Mijalkov, M. & Volpe, G. Sorting of chiral microswimmers. *Soft Matter* **9**, 6376 (2013).
44. Fakhrullin, R. F., Zamaleeva, A. I. & Minullina, R. T. Cyborg cells : functionalisation of living cells with polymers and nanomaterials. *Chem. Soc. Rev.* **41**, 4189–4206 (2012).
45. Fakhrullin, R. F. & Lvov, Y. M. "Face-Lifting" and "Make-Up" for Microorganisms: Layer-by-Layer Polyelectrolyte Nanocoating. *ACS Nano* **6**, 4557–4564 (2012).
46. Kahraman, M. & Zamaleeva, A. I. Layer-by-layer coating of bacteria with noble metal nanoparticles for surface-enhanced Raman scattering. *Anal. Bioanal. Chem.* **395**, 2559–2567 (2009).
47. Niidome, T., Nakashima, K., Takahashi, H. & Niidome, Y. Preparation of primary amine-modified gold nanoparticles and their transfection ability into cultivated cells. *Chem. Commun. (Camb).* 1978–1979 (2004). doi:10.1039/b406189f
48. Kim, Y. *et al.* Stretchable nanoparticle conductors with self-organized conductive pathways. *Nature* **500**, 59–63 (2013).
49. Khlebtsov, N. G. Determination of size and concentration of gold nanoparticles from extinction spectra. *Anal. Chem.* **80**, 6620–6625 (2008).
50. Liu, X., Atwater, M., Wang, J. & Huo, Q. Extinction coefficient of gold nanoparticles with different sizes and different capping ligands. *Colloids Surfaces B Biointerfaces* **58**, 3–7 (2007).
51. Nikoobakht, B. & El-sayed, M. A. Preparation and Growth Mechanism of Gold Nanorods (NRs) Using Seed-Mediated Growth Method. *Chem. Mater.* **15**, 1957–1962 (2003).
52. Liu, P. Y. *et al.* Real-Time measurement of single bacterium's refractive index using optofluidic immersion refractometry. *Procedia Eng.* **87**, 356–359 (2014).
53. Johnson, P. B. & Christy, R. W. Optical constants of the noble metals. *Phys Rev B* **6**, 4370–4379 (1972).
54. Epps, S. V. R. *et al.* Foodborne Campylobacter: Infections, metabolism, pathogenesis and reservoirs. *Int. J. Environ. Res. Public Health* **10**, 6292–6304 (2013).
55. Altekruse, S. F., Stern, N. J., Fields, P. I. & Swerdlow, D. L. Campylobacter jejuni - An emerging foodborne pathogen. *Emerg. Infect. Dis.* **5**, 28–35 (1999).
56. Park, J. H., Hong, D., Lee, J. & Choi, I. S. Cell-in-Shell Hybrids: Chemical Nanoencapsulation of Individual Cells. *Acc. Chem. Res.* **49**, 792–800 (2016).
57. Seisenbaeva, G. A. *et al.* Biomimetic Synthesis of Hierarchically Porous Nanostructured Metal Oxide Microparticles-Potential Scaffolds for Drug Delivery and Catalysis. *Langmuir* **26**, 9809–9817 (2010).
58. Lee, J.; Govorov, A.O.; Dulka, J.; Kotov, N.A. Bioconjugates of CdTe Nanowires and Au Nanoparticles: Plasmon-Exciton Interactions, Luminescence Enhancement and Collective Effects, Nano Lett., 4(12), 2323–2330 (2004).
59. Guerrero-Martínez, A. *et al.* Intense optical activity from three-dimensional chiral ordering of plasmonic nanoantennas. *Angew. Chem. Int. Ed. Engl.* **50**, 5499–503 (2011).
60. Tarantola, M. *et al.* Toxicity of gold-nanoparticles : Synergistic effects of shape and surface functionalization on micromotility of epithelial cells. *Nanotoxicology* **5**, 254–268 (2011).
61. Hajipour, M. J. *et al.* Antibacterial properties of nanoparticles. *Trends Biotechnol.* **30**, 499–511 (2012).
62. Cha, S.-H. *et al.* Shape-Dependent Biomimetic Inhibition of Enzyme by Nanoparticles and Their Antibacterial Activity. *ACS Nano* **9**, 9097–9105 (2015).
63. French, S., Cote, J.-P., Stokes, J. M., Truant, R. & Brown, E. D. Bacteria getting into shape : Genetic determinants of E. coli Morphology. *MBio* **8**, e01977-16 (2017).
64. Young, K. D. Bacterial morphology : Why have different shapes ? *Curr. Opin. Microbiol.* **10**, 596–600 (2007).
65. Cabeen, M. T. & Jacobs-Wagner, C. Bacterial cell shape. *Nat. Rev. Microbiol.* **3**, 601–610 (2005).
66. Choi, W. J. *et al.* Terahertz circular dichroism spectroscopy of biomaterials enabled by kirigami polarization modulators. *Nat. Mater.* **18**, 829–826 (2019).

Graphical Abstract

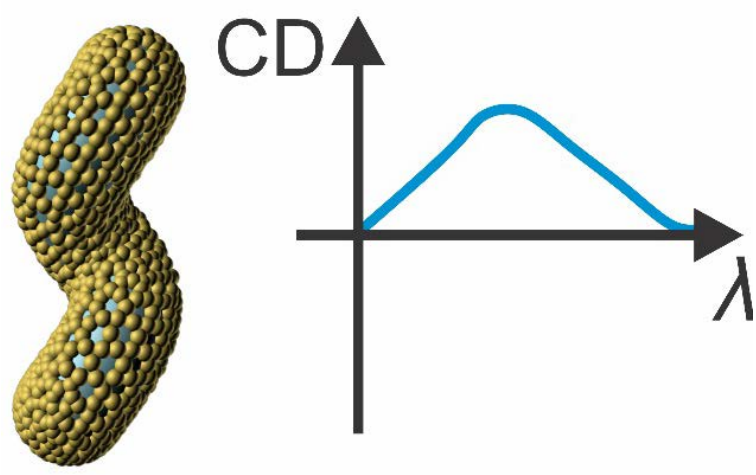

Gold nanoparticles assemble onto the surface of helical bacterium, *Campylobacter jejuni*, producing right-handed helices with a pitch of 1–2 microns. The bacterial dispersion acquires chiroptical activity at 500–750 nm that matches the calculated chiroplasmonic spectra. This study provides a pathway to utilize chiroplasmonic particles for monitoring shape dynamics of bacteria and identification of helical bacteria in complex microbiomes.

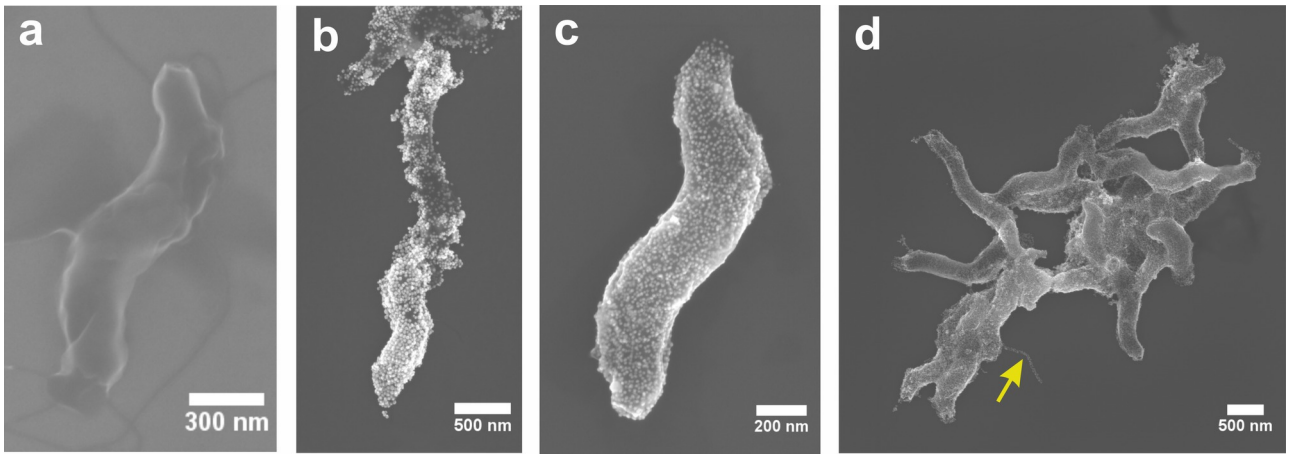

CHIR_23225_Fig 1.jpg

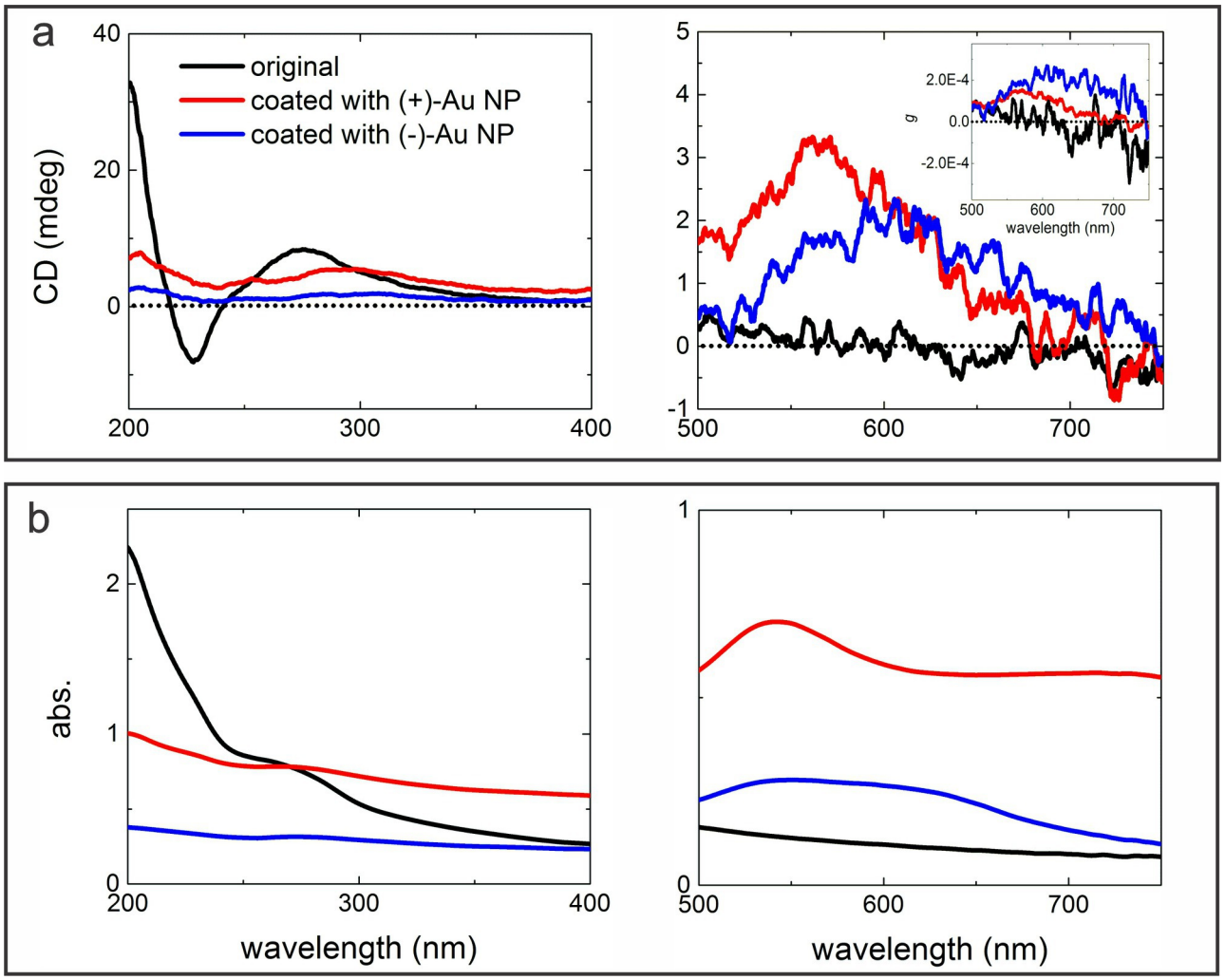

CHIR_23225_Fig 2.jpg

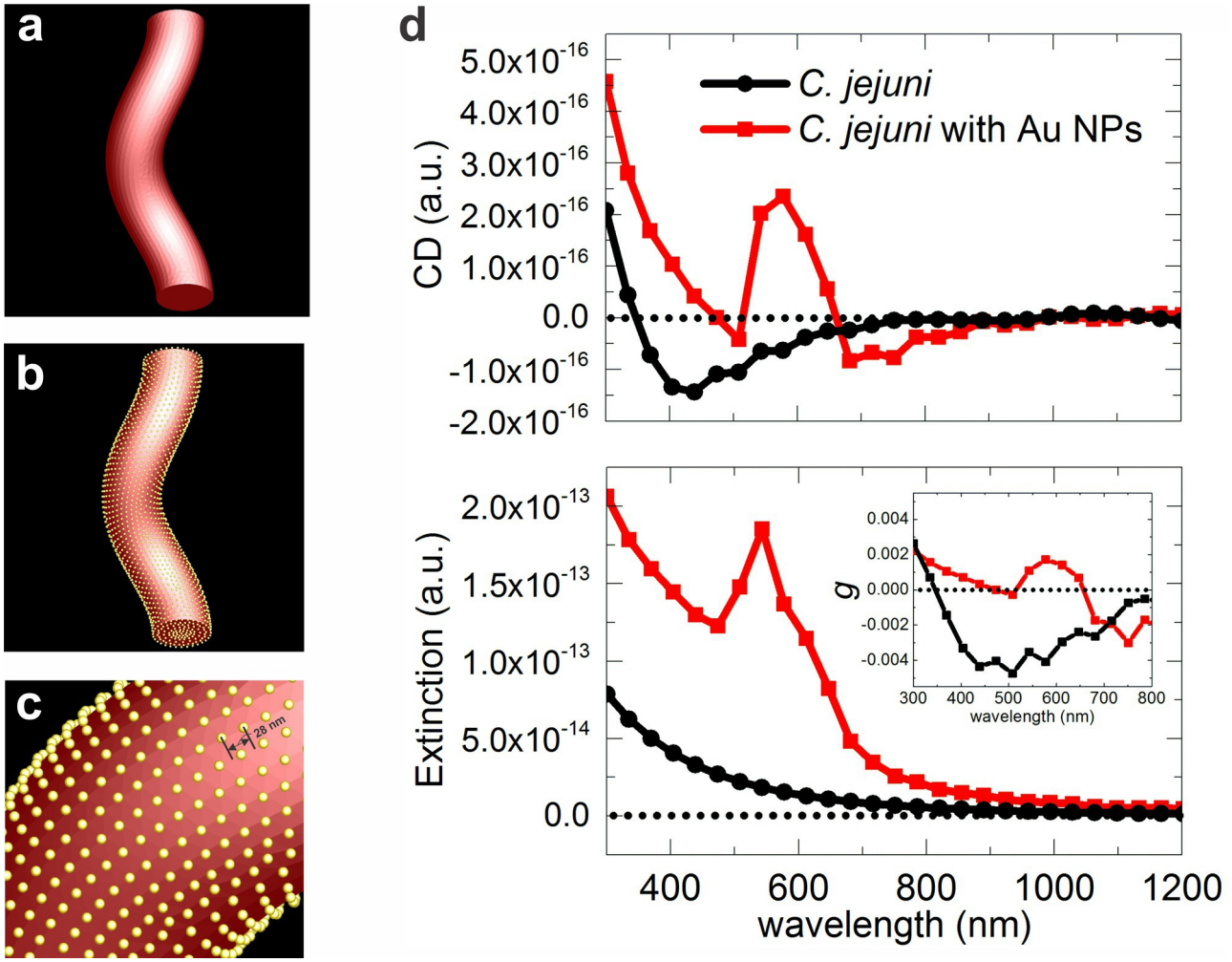

CHIR_23225_Fig 3.jpg